Catalysis Letters
https://doi.org/10.1007/s10562-020-03500-9

Catalytic Conversion of Tetrahydrofurfuryl Alcohol over Stable Pt/MoS_2 Catalysts

Xinsheng Li[1,2] · Jifeng Pang[1] · Wenhao Luo[1] · Yu Zhao[1] · Xiaoli Pan[1] · Mingyuan Zheng[1]

Received: 30 August 2020 / Accepted: 12 December 2020

Abstract

MoS_2 supported noble metal catalysts were used for the catalytic conversion of terahydrofurfuryl alcohol (THFA) to 1,5-pentanediol (1,5-PDO) and its derivate tetrahydropyrane (THP). Over the optimal 4%Pt/MoS_2-FR catalyst, 75.8% overall selectivity (35.4% to 1,5-PDO and 40.4% to THP) and 63.7% conversion of 5 wt% THFA solution were obtained after 8 h reaction at 250 °C. The catalyst showed stable catalytic performance in five-cycle reactions, demonstrating the robustness of Pt/MoS_2 under the harsh hydrothermal and hydrogenation conditions. A variety of characterizations, including CO-DRIFTS, HRTEM, H_2-TPR, Raman spectroscopy and XPS revealed that typical behavior of strong metal-support interaction (SMSI) existed between Pt and MoS_2, largely caused by the coverage of MoS_2 over Pt and rarely reported previously. The Pt/MoS_2 had intact structure under the harsh conditions thanks to the SMSI and chemical stability of MoS_2. The acidity of Pt/MoS_2 was negligible, and the active sites for the reaction were attributed to Pt and the Mo sites interacting closely on the catalysts. The reaction pathway was proposed according to the product distributions and the results of conditional experiments.

Supplementary Information The online version contains supplementary material available at https://doi.org/10.1007/s10562-020-03500-9.

✉ Mingyuan Zheng
myzheng@dicp.ac.cn

[1] CAS Key Laboratory of Science and Technology on Applied Catalysis, Dalian Institute of Chemical Physics, Chinese Academy of Sciences, 457 Zhongshan Road, Dalian 116023, China

[2] University of Chinese Academy of Sciences, 19A Yuquan Road, Beijing 100049, China

Published online: 16 January 2021

Graphic Abstract

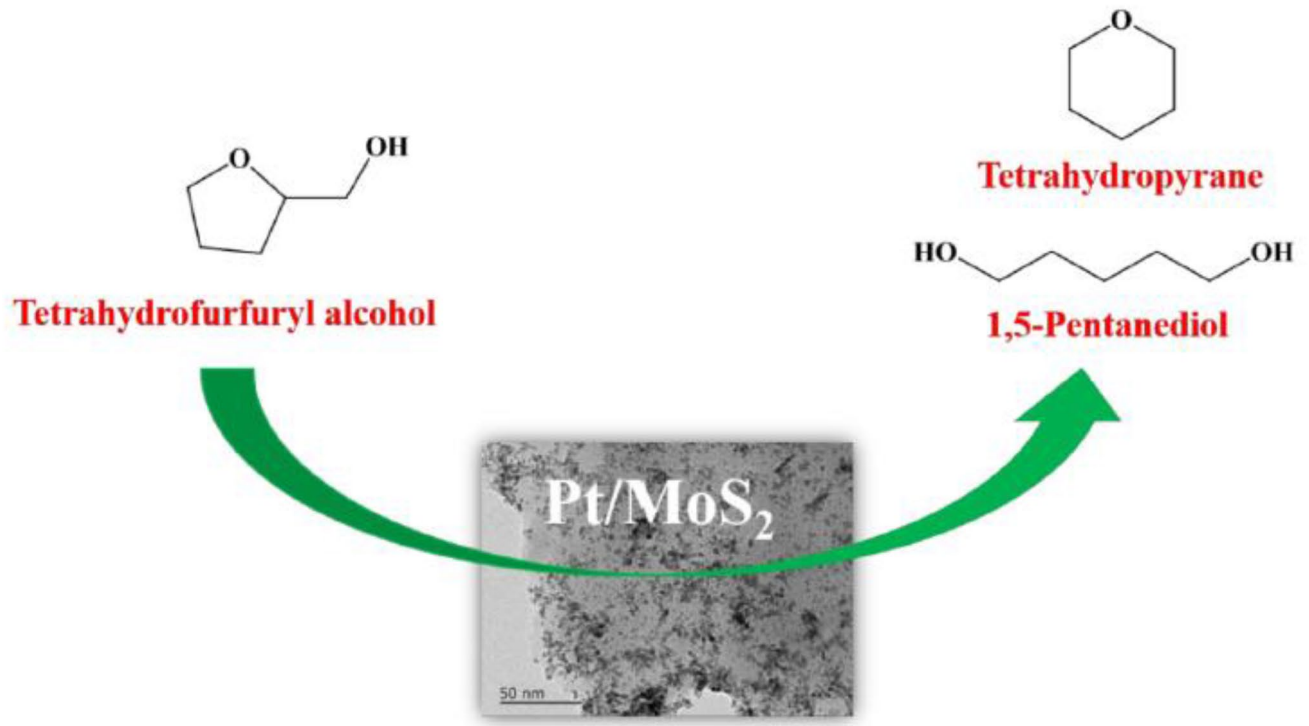

Keywords Tetrahydrofurfuryl alcohol · Platinum · Molybdenum disulfide · Pentanediol · Tetrahydropyrane · Strong metal-support interaction

1 Introduction

The concerns on the limited fossil energy resources and sustainable development of economy have stimulated the extensive investigations on catalytic conversion of biomass to fuels [1–3] and value-added chemicals [4–8]. 1,5-Pentanediol (1,5-PDO) and its derivate tetrahydropyrane (THP) are important chemicals [9, 10], widely used in the synthesis of polyesters, polyurethanes, lubricants, perfumes and advanced solvents [11–13]. For bio-based 1,5-PDO preparation, great efforts have been made in catalytic conversion of the furfural derived feedstocks [14–22]. Tetrahydrofurfural alcohol (THFA) is a total hydrogenation product readily obtained from furfural conversion [23, 24]. A representative process for 1,5-PDO synthesis is hydrogenolysis of THFA by using bifunctional (NM-MOx) catalysts (NM = Rh, Ir, Pt, Ru; M = V, Mo, W, Re) [20, 25–30]. In the one-pot process, the noble metals in the catalysts take charge of activating the hydrogen for hydrogenation, while the transition metal oxides play critical roles in the reactant adsorption and C-O bond activation [28]. For instance, Koso et al. developed the Rh-ReOx/SiO_2 catalyst for the hydrogenolysis of THFA, and obtained > 75% yield of 1,5-PDO after 24 h reaction [20]. Similarly, Ir-VOx/SiO_2, Ir-Mox/SiO_2, and Rh-MoOx/SiO_2 catalysts were developed for this reaction, which provided ca. 90% 1,5-PDO selectivity thanks to the synergistic catalysis between metal and oxide catalysts [31, 32]. On the other hand, due to the detrimental effect of hydrothermal conditions which is widely adopted in the catalytic hydrogenolysis of THFA, the leaching of MOx components on the catalysts readily happens and results in the low stability of catalyst in long time run. It is highly desirable to explore novel robust catalysts which are endurable to hydrothermal and hydrogenation environments for the biomass conversion.

Molybdenum disulfide (MoS_2) is a layered transition metal dichalcogenide successfully used in the hydrogen transferring reactions [33] and those conducted at high temperatures over 300 °C [34]. In addition, it has hydrophobic surface [33], which may contribute to the stable performance under hydrothermal conditions [35]. Motivated by these features, we employed MoS_2 to support different metals for the catalytic conversion of THFA. Over the optimal 4%Pt/MoS_2 catalyst, reasonable selectivity to 1,5-PDO and THP was obtained, and the catalysts showed the high stability. More interestingly, typical behavior of strong metal-support interaction (SMSI) between Pt and MoS_2 was first observed

according to a variety of characterizations, which is rarely reported in literature. According to comprehensive characterizations and analysis, the catalytic active sites on Pt/MoS_2 were discussed. Finally, the reaction pathway was proposed according to the conditional experiments and product distributions. This study may provide new knowledge about properties of MoS_2 supported noble metal catalysts and their application for hydrogenolysis of biomass under harsh hydrothermal conditions.

2 Experimental

2.1 Catalysts Preparation

All the chemicals were of analytical grade and used without further purification. M/MoS_2 (M = Pt, Pd, Ir, Rh and Ru) catalysts were prepared by an incipient-wetness impregnation method. In detail, MoS_2 samples were impregnated with an aqueous solution containing designed amount of metals, and then aged at 25 °C for 12 h, dried at 120 °C overnight and calcinated at 300 °C for 3 h. Before used, the catalyst was reduced at 300 °C in hydrogen flow for 1 h. For the synthesis of Pt/MoS_2/MO_X (M = Ti, Ce, Zr) catalysts, MoS_2/MOx was first prepared by the deposition method as Hu et al. reported [36]. Then, the as-prepared MoS_2/MOx was used as the support for the impregnation process as mentioned above. The obtained catalysts were denoted as Pt/MoS_2/MOx. 4%Pt/MoS_2-FR was prepared by the liquid phase reduction method with formaldehyde as the reductant [37]. In detail, the H_2PtCl_6 solution and MoS_2 were added into a flask under magnetic stirring, followed by the addition of stoichiometric formaldehyde reagent. After adjusting the pH of suspension to 9.0 with 5 wt % NaOH solution and keeping at 50 °C for 1 h, the catalyst was filtered, washed three times with deionized water and dried at 100 °C for 12 h.

2.2 Catalyst Characterization

X-ray diffraction (XRD) patterns of catalysts were obtained on a PW 3040/60 X'Pert PRO (PANalytical) diffractometer equipped with a Cu Kα radiation source (λ = 0.15432 nm) operating at 40 kV and 40 mA. A continuous mode was used in the 2θ range from 10° to 80° at a scanning speed of 5°/min.

Brunauer–Emmett–Teller (BET) surface areas of catalysts were measured using Micromeritics Chemisorb 2720 under the liquid nitrogen temperature after the pre-treatment at 250 °C for 3 h.

The Pt loading and the metal leaching of catalysts were measured by inductively coupled plasma-optical emission spectroscopy (ICP–OES) IRIS Intrepid II.

Thermogravimetric (TG) analysis was conducted with SDT Q600 equipment under air flow from 30 to 900 °C at a heating rate of 10 °C/min.

Transmission electron microscopy (TEM) images of the catalysts were obtained from JEM-2100F at 200 kV. Before characterization, the sample was dispersed in ethanol under ultrasonic for 10 min. A drop of the prepared suspension was then deposited on a Cu grid coated with a carbon layer, and the grid was dried under infrared lamp. High Resolution Transmission Electron Microscopy (HRTEM) images were obtained from JEM-AFM2000F.

CO-diffuse reflectance infrared Fourier transform spectra (CO-DRIFTS) were collected with BRUKER Equinox 70 spectrometer equipped with a MCT detector and operated at a resolution of 4 cm^{-1} and 32 scans. The samples were pretreated with 5% H_2/He at 180 °C for 1 h, followed by purging with He at 180 °C for 10 min. After the temperature decreased to the experiment temperature (25 °C or − 120 °C), the background spectrum was collected. Then CO flow was introduced for 10 min to reach the CO saturated adsorption. Again, the gas was changed to He flow, and after 20 min the spectra of CO adsorbed were collected.

X-ray photoelectron spectroscopy (XPS) of catalyst was measured on Thermofisher ESCALAB 250Xi. The Monochromated AlKα source was operated at hυ = 1486.6 eV, 15 kV and d 10.8 mA. All samples were pre-treated by 5% H_2/He at 180 °C for 1 h. C 1 s, Pt 4f, Mo 3d, S 2 s and S 2p signals were obtained. Binding energy (BE) values were referenced to the binding energy of the C 1 s core level at 284.6 eV.

2.3 Catalytic Reaction

Catalytic conversion of THFA was performed in a 50 mL hastelloy autoclave. In a typical experiment, 5 wt% aqueous THFA (totally ca. 20 g) was loaded into the reactor with 0.1 g catalyst. Then, the autoclave was sealed and purged with H_2 for 3 times to exclude air. After 4 MPa H_2 was charged into the reactor, the reaction was conducted at desired temperature for 8 h with magnetic stirring at 800 rpm.

2.4 Analytical Method

The liquid products were analyzed by using GC (gas chromatograph, Agilent, 7890 B) equipped with a FFAP column and a flame ionization detector (FID). Hexanol was used as the internal standard. The gaseous products were collected and analyzed by a GC equipped with an Al_2O_3 column and a thermal conductivity detector (TCD).

3 Results and Discussion

3.1 Thermal Stability of MoS_2 Support

Considering the catalytic conversion of THFA is usually conducted under hydrothermal reduction conditions which may cause oxidation or hydrogenolysis of metal sulfides, we first evaluated the thermal stability of MoS_2 and its supported noble metal catalysts by TG in air. As shown in Fig. 1a, no weight loss was observed below 350 °C for MoS_2. The major peaks on the thermal profile appeared at 521 °C and 825 °C, corresponding to the partial and complete oxidation of MoS_2 at high temperatures, respectively. Noble metals are reported to catalyze oxidation reactions [38–41]. For the MoS_2 supported noble metal catalyst 4%Pt/MoS_2 (Fig. 1b), the presence of Pt slightly decreased the oxidation temperature to 373 °C, still highter than that in most hydrothermal conditions for biomass conversion. This indicates that the loading of Pt on MoS_2 did not ruin the anti-oxidation capability of the catalyst. Similarly phenomenon was also observed on the 4%Pd/MoS_2 catalyst (Fig. S1a). Therefore, the MoS_2 supported noble metal catalysts would be able to endure the oxidation conditions in a wide range of reaction temperatures.

The stability of MoS_2 and 4%Pt/MoS_2 catalyst in hydrogen atmosphere was evaluated by H_2-TPR experiments. As shown in Fig. 2, MoS_2 was hardly reduced by H_2, and merely very weak reduction peaks appeared at 292 °C and 381 °C. For the supported catalyst 4%Pt/MoS_2, several reduction peaks present in a wide range of temperature from -17 °C to 827 °C, and the major reduction peak appeared at 352 °C. Referring to the reduction behavior of MoS_2, the peaks below 350 °C should be largely attributed to the reduction of Pt [42]. Taken together, MoS_2 is an ideal support to load noble metals for the catalytic hydrogenolysis of THFA that is usually conducted below 300 °C.

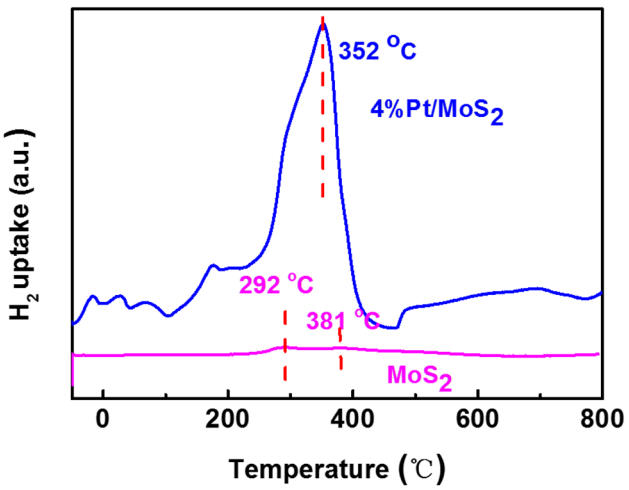

Fig. 2 H_2-TPR profiles of MoS_2 support and 4%Pt/MoS_2

3.2 Catalytic Conversion of THFA Over Different Catalysts

3.2.1 Different Noble Metal Catalysts

We first screened the catalytic performance of different noble metals loaded on MoS_2 in the THFA conversion. As shown in Table 1, among various noble metal catalysts, 4%Pt/MoS_2 catalyst is the distinguished one. It gave 1,5-PDO and THP products with total selectivity of 55% (35.0% to 1,5-PDO and 20.2% to THP) at 41.2% THFA conversion. The reaction selectivity is rather different from that obtained over the NM-MOx catalysts reported previously, where 1,5-PDO but no THP was obtained as a major product [31, 32]. Over other noble metal catalysts, including Ir, Rh and Pd loaded on MoS_2, the 1,5-PDO and THP selectivities were much lower (< 20%, Table 1, Entries 2–4). The carbon balances in these reactions are also very low, and most byproducts are undetectable by GC (Fig. S2). This should be attributed to the large molecule humins formation, as reflected by the color of reaction solution changing from clear to brown, or the formation of sticky materials adhering to the stirring paddle in the reactor after reaction. Thus, our study focused on the Pt/MoS_2 catalyst in the following sections.

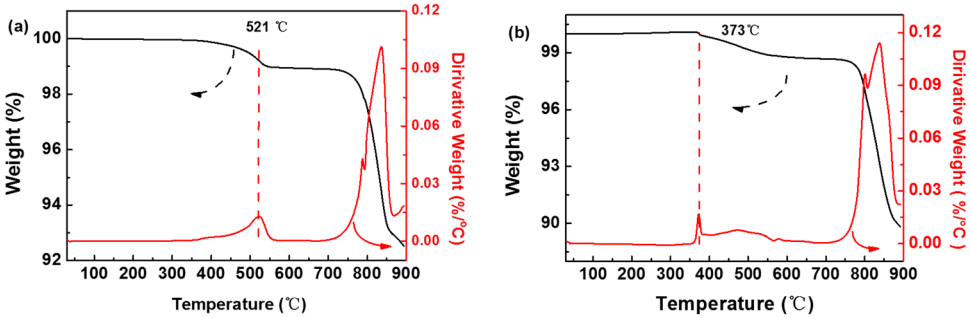

Fig. 1 TG analysis of (**a**) MoS_2 support and (**b**) 4%Pt/MoS_2 catalyst in air

Table 1 Results of THFA conversion over various MoS_2 supported metal catalysts

Entry	Catalyst	Conv./%	Selectivity/%				
			1,5-PDO	THP	MTHF	Pol	Pe
1	4%Pt/MoS_2	41.2	35.0	20.2	2.2	4.0	1.6
2	4%Ir/MoS_2	12.4	15.4	Trace	Trace	Trace	1.7
3	4%Rh/MoS_2	17.8	17.3	Trace	Trace	Trace	0.4
4	4%Pd/MoS_2	11.8	17.5	Trace	Trace	Trace	0.3
5	1%Pt/MoS_2	1.8	84.2	Trace	Trace	8.2	4.5
6	2%Pt/MoS_2	3.2	72.6	Trace	Trace	7.6	3.7
7	6%Pt/MoS_2	22.1	51.9	10.4	2.1	4.2	–
8	8%Pt/MoS_2	10.5	57.4	Trace	Trace	4.2	–
9	4%Pt/MoS_2-FR[b]	63.7	35.4	40.4	3.5	4.3	0.1
10	4%Pt/MoO_3	77.1	14.0	3.7	3.2	2.3	ND

[a]Reaction conditions: 20 g 5 wt% THFA aqueous solution, 0.1 g catalyst, 4 MPa H_2, 250 °C, 8 h; Trace: less than 0.1%; ND: not detected. Conv., 1,5-PDO, THP, MTHF, Pol and Pe are abbreviations for conversion, 1,5-pentanediol, tetrahydropyrane, 2-methyl tetrahydrofuran, 1-pentanol and pentane, respectively

[b]The catalyst was prepared by the formaldehyde reduction method

3.2.2 Effect of Pt Loading on the Reaction

The Pt loading on the catalysts showed remarkable influence on the reaction, as shown in Table 1, Entries 1, 5–8. At 1 wt% Pt loading, the THFA conversion was as low as 1.5% but with high selectivity of 1,5-PDO up to 84.2%. Doubling the Pt loading to 2 wt% slightly improved the THFA conversion to 3.2%. In contrast, when further increasing the Pt loading to 4 wt%, the THFA conversion was drastically enhanced by one order of magnitude (41.2%). On the other hand, the reaction selectivity shifted from the dominated 1,5-PDO product to 1,5-PDO and THP. The drastic changes in the reaction activity and selectivity suggest that the quantity and the property of catalytic sites were altered at different Pt loadings. Further increasing the Pt loading to 6 ~ 8 wt% led to a depressed THFA conversion, which should be ascribed to the decreased dispersion of Pt over MoS_2 at higher metal loadings, as evidenced by the TEM images discussed below. More discussion about metal loading effect was provided in Sect. 3.4.

3.2.3 Pt Dispersion and the Stability of Catalysts

Reducing catalyst under mild conditions could contribute to generating metal particles in uniform size and improving the number of active sites on the catalyst support [43, 44]. Therefore, we employed an aqueous formaldehyde reduction (FR) method to synthesize 4%Pt/MoS_2-FR catalyst. From the TEM images (Fig. 3a, Fig. S3), it can be confirmed that the Pt particles on the as-prepared 4%Pt/MoS_2-FR had more uniform sizes (3–4.5 nm vs 2–5 nm) as compared with that prepared by H_2 reduction at a high temperature. The EDS mapping (Fig. 3c) shows that Pt, Mo and S were uniformly distributed, confirming the high dispersion of Pt on MoS_2 prepared by the FR method. The 4%Pt/MoS_2-FR was used in the THFA conversion, and achieved 63.7% THFA conversion and 76.2% overall selectivity of the target products (35.0% to 1,5-PDO and 41.2% to THP, Table 1, Entry 9), which are much higher than that of the counterparts prepared by H_2 reduction.

In view of the low specific surface area of the commercial MoS_2 (5.1 m^2/g), we attempted to load MoS_2 on some oxide supports with larger surface areas, including TiO_2, CeO_2 and ZrO_2, and then load Pt to further improve the catalytic performance. Unfortunately, compared to the MoS_2 supported catalyst, the as-prepared composite catalysts did not show enhancement in the catalytic performance although the specific surface areas were enlarged by 3–4 times (Table S1). This suggests that Pt has already been highly dispersed on MoS_2 even the MoS_2 support has rather low surface areas, which is consistent with the TEM observation as mentioned above.

Then, the stability of MoS_2 supported catalyst in the reaction was evaluated over the optimal 4%Pt/MoS_2-FR. As shown in Fig. 4, after five consecutive runs at 250 °C in water for 8 h, the overall selectivity to 1,5-PDO (> 30%) and THP (ca. 40%) was kept at 67–75% and the THFA conversion was maintained at 55–65%. The slight decrease in the activity may be caused by the weigh loss of catalysts during the catalyst recycling. The amount of metals and sulfur leaching into the reactant solution were analyzed by ICP-OES. Consistent to the thermal analysis of MoS_2 in Fig. 1 and 2, no Mo and merely 0.99% of sulfur was detected in the solution after reaction (Table S2), and the amount of Pt leaching was also negligible (account for 0.02% of Pt loaded on the catalyst). Therefore, the 4%Pt/MoS_2-FR catalyst was proved to show stable catalytic performance and well

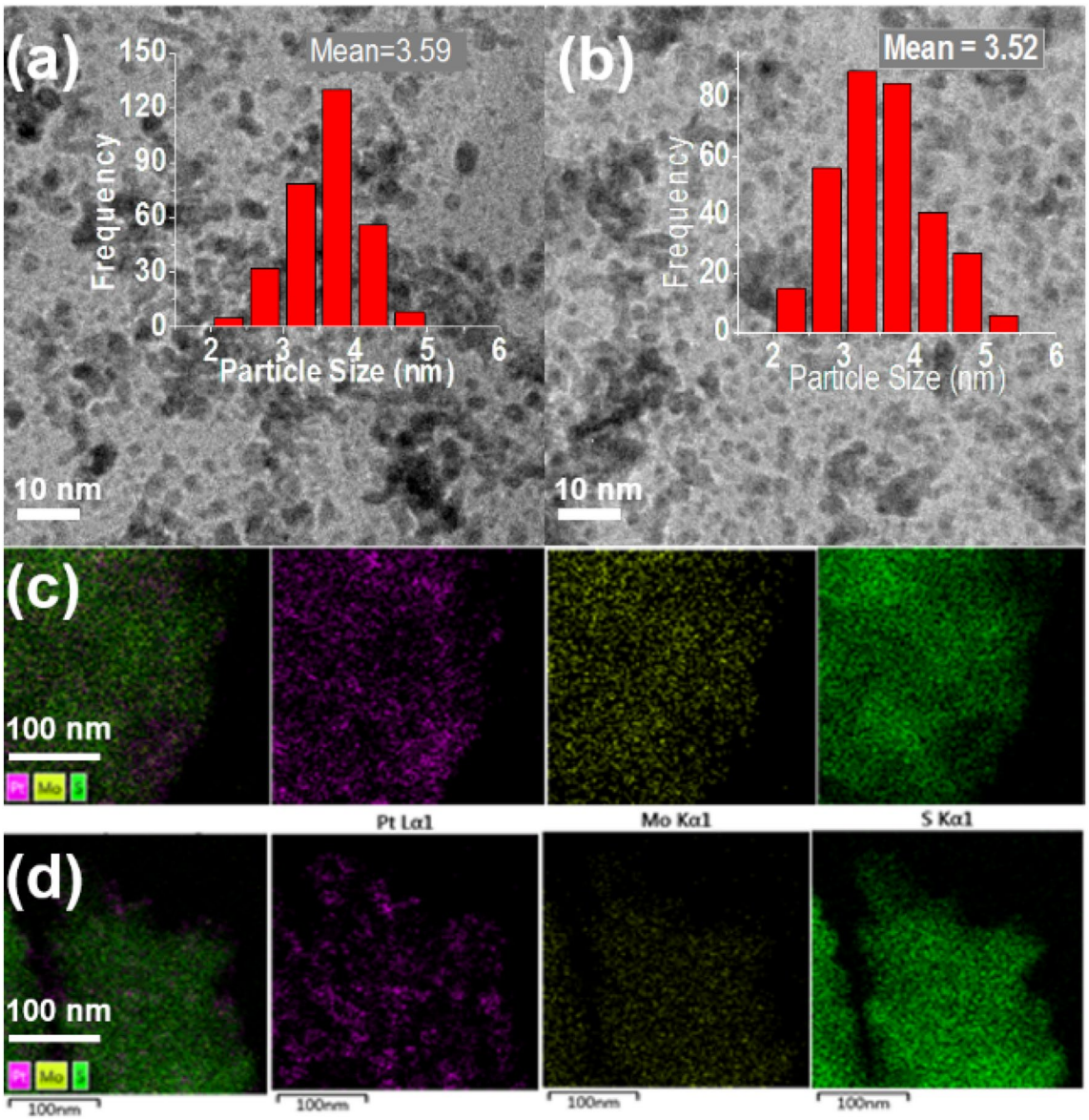

Fig. 3 TEM and EDS images of (**a**), (**c**) 4%Pt/MoS_2-FR-Fresh and (**b**), (**d**) 4%Pt/MoS_2-FR-Spent catalysts

retain the active components under the present harsh reaction conditions.

In summary, MoS_2 supported Pt catalysts showed reasonable activity and highly stable performance in THFA hydrogenolysis to 1,5-PDO and THP under 250 °C hydrothermal hydrogenation conditions. The catalytic results were strongly affected by the Pt loading on MoS_2. In the following sections, we characterized the Pt/MoS_2 catalysts by using a variety of methods, trying to unveil the unique properties of the MoS_2 supported noble metal catalysts and their effects on the catalytic performance.

3.3 Physicochemical Properties Characterization of Pt/MoS_2 Catalysts

3.3.1 XRD Patterns and TEM Images

The crystalline structure of Pt/MoS_2 catalysts was analyzed by XRD. As shown in Fig. 5, except the peaks ascribed to the crystalline MoS_2, no peak assigned to metallic Pt was observed over the 1%- 8% Pt/MoS_2 catalysts. This indicates that Pt may be highly dispersed on the MoS_2 support. For the spent 4%Pt/MoS_2-FR, also no

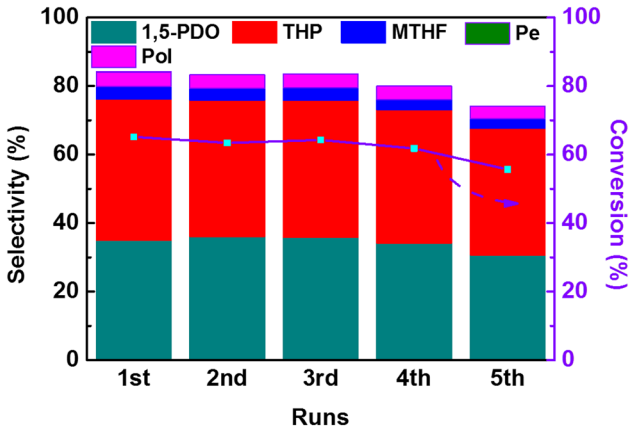

Fig. 4 Reusability of the 4%Pt/MoS_2-FR catalyst in THFA conversion (Reaction conditions: 20 g 5 wt% reactant aqueous solution, 0.1 g catalyst, 4 MPa H_2, 250 °C, 8 h)

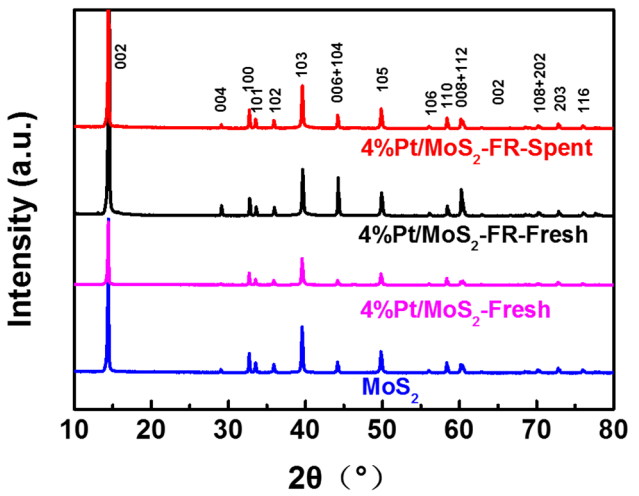

Fig. 5 XRD patterns of the MoS_2 support and 4%Pt/MoS_2 catalysts

crystalline change was found, reflecting the good stability of the catalyst.

TEM images reveal the distribution of metallic Pt nanoparticles on the MoS_2 (Fig. S3). For the Pt/MoS_2 catalysts with 1 ~ 4 wt% Pt loadings, there is no substantial difference in the averaged Pt particle size, which varied from 1.7 nm to 3.4 nm. Correlating to the ten-time enhancement in the catalytic activity with Pt loading increase as mentioned above, it is hard to believe that such significant difference in the catalytic performance was merely caused by the different size of metallic nano particles. There may be some other reasons to account it. Further increasing Pt loading to 6 wt% and 8 wt% led to remarkable agglomeration of metal particles, which may explain the decrease of catalytic activity at high Pt loadings.

The 4%Pt/MoS_2-FR catalyst samples before and after reaction were compared in TEM analysis. As shown in Fig. 3a, b, the Pt particle sizes were retained well after the catalyst five-cycle runs, confirming the high stability of the Pt/MoS_2 catalyst under hydrothermal hydrogenation conditions. At higher resolutions, HRTEM images (Fig. 6) show that besides a large number of Pt particles in a size of ca. 3 nm loaded on MoS_2 nanosheets, some Pt particles were covered by thin layers of MoS_2. Moreover, some Pt single atoms were found to be embedded into the MoS_2 layer around the Pt nano particles. Over the spent catalyst, the coverage of MoS_2 on the Pt nanoparticles is more apparent, possibly due to the enhancement by the high temperature for the reaction. According to the studies by Liu and Qiao et al., SMSI can make support encapsulate the metallic particles [45, 46]. The readily coverage of Pt particles by MoS_2 observed herein suggests that the SMSI was possibly present over the Pt/MoS_2 catalysts, even under mild preparation conditions (formal aldehyde reduction was performed at 50 °C, and then sample was dried at 120 °C in air).

3.3.2 H_2 and CO Adsorption Measurement

To further identify the SMSI and unveil its effects on the catalyst properties, we conducted H_2 and CO adsorption measurement on the 4%Pt/MoS_2 catalyst. It was found that the quantities of the probing molecules adsorbed were nearly undetectable at ambient temperatures, even though a high loading of Pt in the catalyst. This indicates that almost no metallic Pt sites were exposed on the catalyst surface, which is quite contrary to the high dispersion of Pt observed in HRTEM images (metal particles with a size of 3 nm in diameter corresponding to ca. 33% metal dispersion). CO-DRIFTS is a more sensitive method than CO-chemosorption for probing the metallic Pt sites. Before the CO adsorption, the catalyst was in-situ reduced at 180 °C in a 5% H_2/He gas flow for 1 h and purged with He to keep catalyst surface fresh and clean. However, the intensity of IR peak owing to CO adsorption on the Pt^0 sites (Fig. S4, 2050 cm^{-1}) is rather low, no matter the adsorption was conducted at room temperature or as low as -120 °C. Over the spent catalyst, the peak of CO indexed to Pt^0 adsorption nearly disappeared. Again, it is manifested that the capability of Pt/MoS_2 to adsorb small probing molecules is quite weak.

It has been widely accepted that as a classic behavior, SMSI drastically suppresses CO or H_2 chemosorption on a catalyst [47, 48]. Therefore, the most plausible explanation to the puzzling phenomena found herein should be the SMSI existing between Pt and MoS_2, which is not reported yet in literature as far as we know. The SMSI could be caused by two means, i.e., electron transferring between Pt and S [49], and the coverage of MoS_2 on Pt particles. This may contribute to catalyst stability [50–52], as well as the high

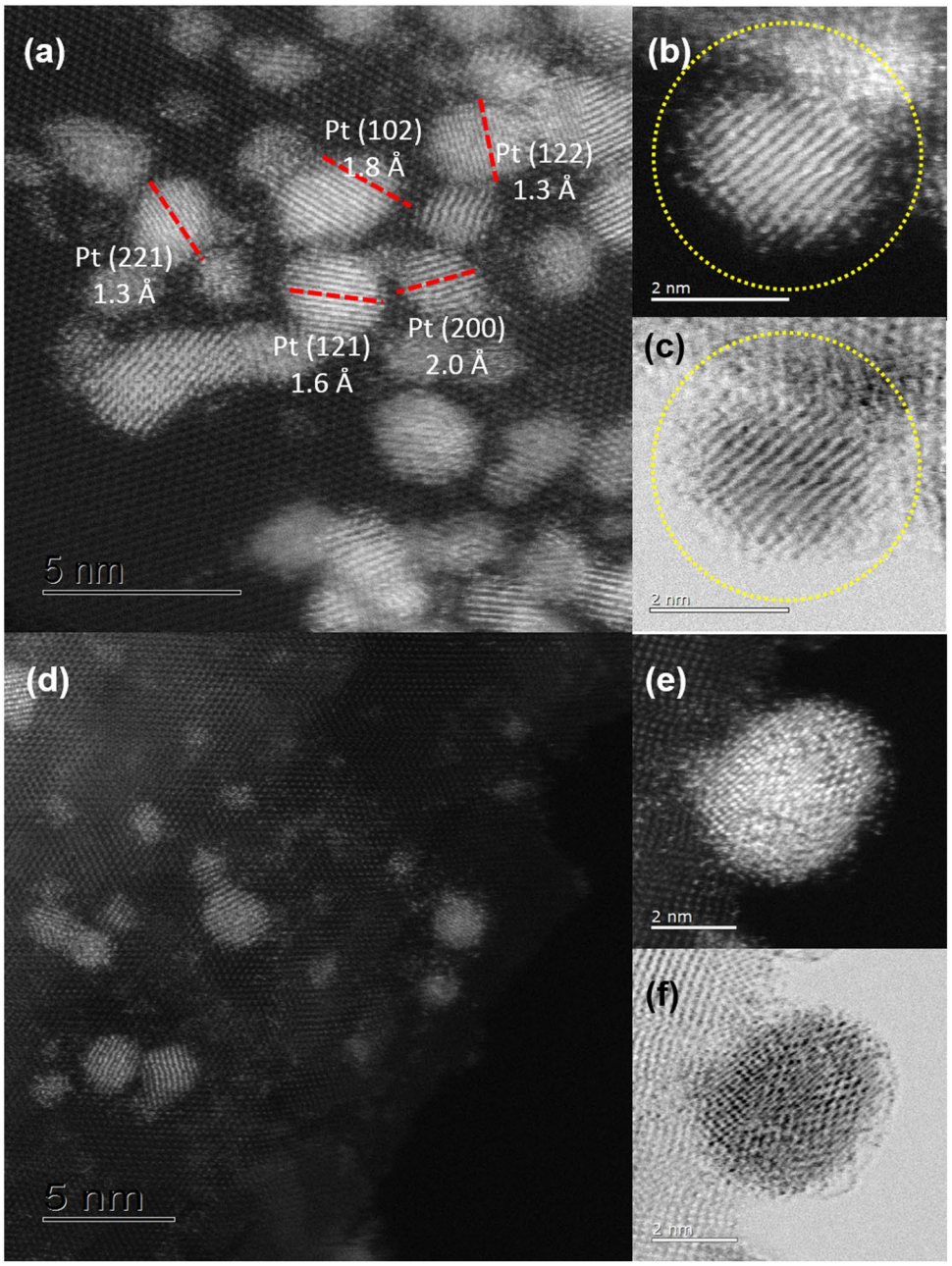

Fig. 6 HRTEM images of (**a**–**c**) 4%Pt/MoS_2-FR-Fresh and (**d**–**f**) 4%Pt/MoS_2-FR-Spent

dispersion of metallic Pt on MoS_2, of which specific surface area is as low as 3.8 m^2/g. On the other hand, the too strong SMSI may depress the catalytic activity, as demonstrated in the cases of 1%-2%Pt/MoS_2.

3.3.3 TPO–TPR Experiments

To discern the interaction between Pt and the MoS_2 support, we conducted TPO-TPR experiments for the catalysts with varied Pt loadings. The Pt/MoS_2 catalysts were pre-oxidized in O_2/N_2 (10 v/v%) at 200 °C for 30 min, based on the consideration that 4%Pt/MoS_2 can endure O_2 oxidation below 372 °C without changing the major phase of MoS_2 (according to the TG–DTA analysis discussed above), and then H_2-TPR experiments were performed. As shown in Fig. 7, four reduction peaks appeared on each of the TPR profiles. On-line MS analysis showed that merely H_2O but no H_2S was detected in the gas products during the H_2-TPR process. This indicates that the reduction peaks should belong to metal oxides reduction. The two peaks below 340 °C seem to be related to the PtOx reduction [42], and the peaks at higher temperatures may belong to MoOx reduction (according to Raman and XPS analysis discussed below, some amount of Mo^{6+} species should locate at the inner position of the

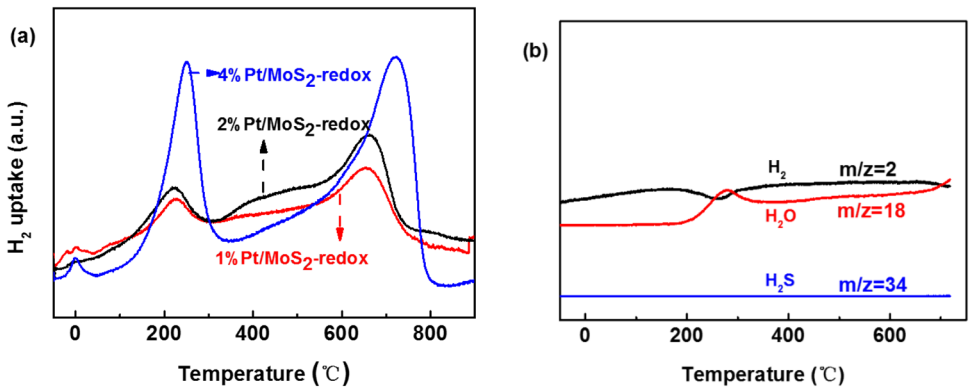

Fig. 7 TPO-TPR profiles of (**a**) 1%Pt/MoS_2, 2%Pt/MoS_2 and 4%Pt/MoS_2; (**b**) MS signal of 4%Pt/MoS_2 during TPR process

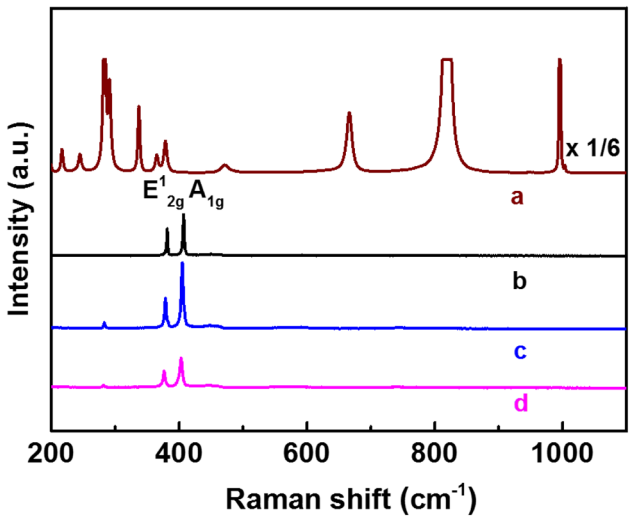

Fig. 8 Raman spectra of (**a**) MoO_3, (**b**) MoS_2, (**c**) 4%Pt/MoS_2-FR-Fresh and (**d**) 4%Pt/MoS_2-FR-Spent

commercial MoS_2). However, the quantification analysis shows that amount of H_2 consumption below 340 °C was two times of that theoretical amount of H_2 consumption for Pt 100% reduction over 4%Pt/MoS_2. Similar phenomena were also found on 1%Pt and 2%Pt/MoS_2 catalysts. The excessive consumption of H_2 should be attributed to MoOx sites derived from MoS_2 oxidation by O_2/N_2 treatment which closely contacted Pt sites. Evidently, the interaction between Pt and MoS_2 activated the Mo sites which contact Pt to serve as catalytic sites for reactions.

3.3.4 Raman and XPS Spectra of Catalysts

The Mo species on 4%Pt/MoS_2 surface were probed with Raman spectroscopy. As shown in Fig. 8, only the peaks belonging to MoS_2 were observed at 383 cm^{-1} and 409 cm^{-1} [53]. No signals of MoO_3 were present, even for the spent 4%Pt/MoS_2. This demonstrates that the Pt/MoS_2 surface did not bear molybdenum oxide, and the MoS_2 support is stable enough to endure the harsh conditions without oxidization by the hot H_2O during the reaction.

XPS characterization further revealed the chemical composition on the Pt/MoS_2 catalysts. As shown in Fig. 9a, the peaks at 71.54 eV and 74.86 eV were attributed to the Pt^0 species [54], accounting for 45.3% of Pt in the catalyst. The peaks at 72.17 eV and 75.43 eV belonged to the PtOx species, which was caused by the catalyst exposure to air during the storage. For the spent catalyst, the percentage of Pt^0 was well retained. As to the Mo 3d spectra shown in Fig. 9b, the major peaks at 229.51 eV and 232.67 eV were attributed to the MoS_2. Additionally, peaks at 233.52 eV and 236.23 eV with lowered intensity were ascribed to Mo^{6+} species, which account for 24.7% of the whole MoS_2 support. Correlating to the Raman spectra where no MoO_3 was observed on the surface of MoS_2, we conjectured that the Mo^{6+} species should locate at the inner position of the commercial bulk MoS_2. After reaction, the percentage of Mo^{6+} decreased slightly, may be related to its partial reduction to Mo^{4+} (it can not be differentiated from MoS_2 by XPS) under hydrogenation conditions. From the XPS survey spectra (Fig. 9c), the O 1s peak intensity relative to that of Mo 3d in the spent catalyst was decreased as compared to that in the fresh catalyst. This indicates that the MoS_2 support has high unti-oxidation capability during the reaction under hydrothermal condition.

In addition, it can be found from the XPS survey spectra, peak intensity of Pt relative to that of Mo 3d in the spent catalyst was decreased by more than five times as compared to that in the fresh catalyst, suggesting Pt content on the catalyst surface decreased remarkably. However, according to the amount analysis of Pt leaching into the reaction solution and the Pt retained in the spent Pt/MoS_2 catalyst, Pt still existed in the catalyst with the intact loading. This strongly suggests that the majority of Pt particles are covered by MoS_2 during the reaction at high temperatures due to the SMSI, which is consistent to the HRTEM images.

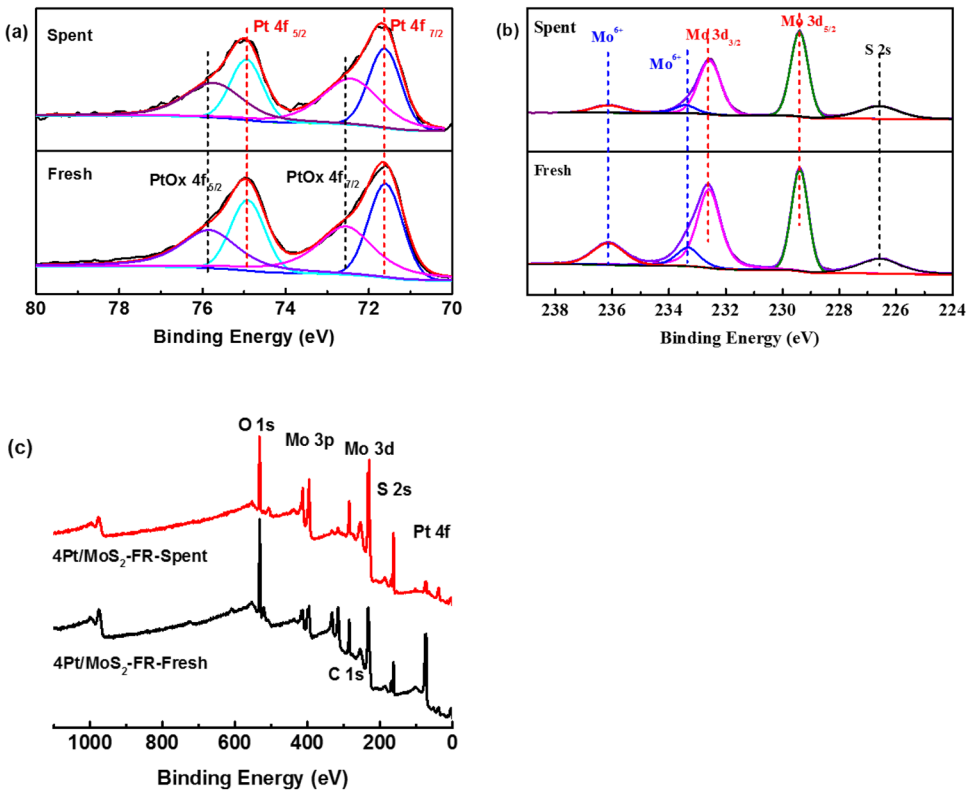

Fig. 9 XPS spectra of 4%Pt/MoS_2-FR before and after reaction (**a**) Pt 4f; (**b**) Mo 3d; (**c**) survey spectra

3.3.5 Acidity of Pt/MoS_2 Catalysts

It is widely proposed that acid sites play important roles in hydrogenolysis C-O containing compounds such as THFA, HMF and glycerol over oxophilic transition metal oxide modified catalysts [29, 32, 55–57]. Therefore, we attempted to measure the acid property of 4%Pt/MoS_2 by using pyridine and 2,6-di-tert butylpyridine (DTBP) FTIR spectroscopy. Unfortunately, no pyridine or DTBP adsorption was observed over 4%Pt/MoS_2, quite differing from the result of pyridine adsorption used to probe the acidity of MoO_3 [58]. This suggests that the acidity of the 4%Pt/MoS_2 catalyst is very weak, if it had, at least lower than that of MoO_3 based catalysts. This is also an evidence for the judgement that no MoOx was present on the catalyst surface. The lack of acid sites on the Pt/MoS_2 catalysts might be one of the reasons why the reaction had to be conducted at a high temperature.

It is reported that noble metal sites can generate protons via H_2 heterolytic dissociation particularly in water solution [57, 59, 60]. The water solvent plays an important role in reducing the proton diffusion barrier and contributes to its spillover [60]. We conducted conditional experiments using different solvents including isopropanol, 1,4-dioxane, or without using of a solvent. Quit differing from the results in water, nearly no 1,5-PDO and THP were formed in these organic solvents, or the conversions of THFA were very low (Table S3). This is consistent with the result obtained by Nakagawa et al. that 1,5-pentanediol production was remarkably depressed when the reaction solvent was shifted from water to n-heptane (an aprotic and nonpolar solvent). The reason was attributed to the difficulty in the formation of anionic hydrogen species in non-polar alkane solvent over Ir-ReOx/SiO_2 [61]. Therefore, we conjectured that H_2 heterolytic dissociation on the Pt/MoS_2 was promoted in water to in-situ generate acid sites, which played the key role in THFA hydrogenolysis.

3.4 Discussion on Active Sites and Catalyst Stability

From the HRTEM and XRD patterns analysis discussed above, there is no substantial difference in the averaged Pt particle size, which varied from 1.7 to 3.4 nm over 1–4%Pt/MoS_2 catalysts. However, the catalytic activity was enhanced by ten times with the Pt loading increase. On the other hand, the quantities of metallic Pt sites on the catalyst were undetectable by the surface sensitive methods like H_2 and CO chemosorption. Some of Pt particles were even found to be covered by MoS_2 layers, which is consistent to the XPS analysis. The TPO-TPR experiments showed that Pt contacted Mo species closely. The SMSI effects evidently occurred on Pt/MoS_2, which are possibly caused by electron transferring between Pt and S [49], and the coverage of MoS_2 on Pt particles. We proposed that the SMSI significantly depressed the activity of Pt particles, particularly for

that with low Pt loadings and particles smaller than 2 nm. Similar effect was also reported on M-WOx/TiO_2 catalysts, of which activities for THFA derivate hydrogonolysis differed by two order magnitude due to the overcoat of support on the noble metal particles (< 2 nm) [62]. In another study reported by Qiao and Li et al. very recently, the size of nano metal particles was found to significantly affect the SMSI on the support, and a larger nano metal particle was more prone to be encapsulated by the support layer than the smaller one owing to the higher surface tension on the former [63]. These results reported in literatures reflect the complexity of SMSI on different materials. Correlating to our study, given the increase of Pt loading from 1 to 4 wt% altered the nano particle size to some extent, it would affect the SMSI on MoS_2 and accordingly changed catalytic performance. The active sites on the Pt/MoS_2 catalyst should be attributed to Mo and Pt sites which interacted closely. The Mo sites activated by the contacted Pt species adsorbed the reactant, and the nearby Pt sites catalyzed the hydrogenation.

As for the acidity, the pyridine and DTBP-FTIR spectroscopy measurements showed that the number of acid sites on the Pt/MoS_2 catalyst before or after reaction is too low to discern. No MoO_3 was observed on the fresh or spent catalyst surface, as shown by Raman spectra and the pyridines-FTIR results. The comparison experiment, where 4 wt% Pt/MoO_3 gave very low the selectivity of 1,5-PDO and THP (15% in total, Table 1, Entry 10), further excluded contribution of MoOx (if there were any) to the reaction over Pt/MoS_2. The solvent effect evaluation shows that water is the distinguished one as compared to other organic solvents. Correlating our study results to the previous studies reported by different research groups worldwide [57, 59–61], we conjectured that the acidic sites over the catalyst required for THFA hydrogenolysis should be the in-situ generated protons, which are generated via heterolytic cleavage of H_2 over Pt sites, further spilled over to the nearby MoS_2 sites with the aid of water, and catalyze the ring opening of the reactant.

The Pt/MoS_2 catalysts showed high stability, without changing the crystalline structure of MoS_2 and no sinter or leaching of Pt on the catalyst. The high stability, one one hand, should be attributed to the essential chemical stability of MoS_2 and Pt under reaction conditions. On the other hand, the SMSI should afford great contribution, particularly to the anti-sintering property of Pt over the MoS_2 support.

3.5 Reaction Route of THFA Conversion

The dependence of catalytic performance on the reaction time was measured over 4% Pt/MoS_2-FR. From the plots shown in Fig. 10 it can be observed that at the low conversion of THFA, the 1,5-PDO selectivity was as high as ca. 80% and continuously decreased to 35% at 8 h. These data

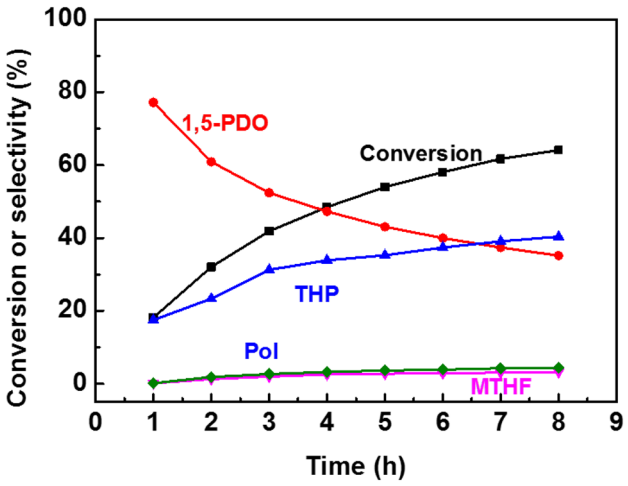

Fig. 10 Results of THFA conversion over 4%Pt/MoS_2-FR at different time. 1,5-PDO, THP, MTHF, and Pol are abbreviations for conversion, 1,5-pentanediol, tetrahydropyrane, 2-methyl tetrahydrofuran, and 1-pentanol, respectively

are consistent to those observed over Pt/MoS_2 catalysts with different Pt loadings (Table 1), where higher 1,5-PDO selectivity was obtained at lower THFA conversions. On the other hand, the THP selectivity gradually increased with reaction proceeding at the expense of 1,5-PDO selectivity dropping, suggesting that 1,5-PDO may be further converted to THP. 1,2,5-pentanetriol (1,2,5-PTO) was supposed to be the reaction intermediate via a minor route for 1,5-PDO formation from furfural alcohol over typical ReOx modified noble metal catalysts [64], however, in our study it was absent in the products in the whole reaction process. This suggests that the 1,5-PDO is less possible to be formed in THFA hydrogenolysis via 1,2,5-PTO as the intermediate, which is in line with the direct hydrogenolysis route proposed by Koso et al. [65].

A set of conditional experiments were performed to further investigate the possible reaction pathways of THFA conversion. The relationship between THP and 1,5-PDO was further investigated in control experiments. As shown in Table 2, Entries 2–3, when THP was used as the feedstock for the reaction, 7.7% selectivity to 1,5-PDO was obtained at 30% conversion of THP. In contrast, when using 1,5-PDO as the feedstock, 66.2% selectivity to THP and 88.5% conversion of 1,5-PDO were obtained. This demonstrates that THP is a more stable product than 1,5-PDO, which is apt to undergo further reaction to THP under the reaction conditions.

Then, we tested the 1,2,5-PTO conversion and obtained 24.5% selectivity to 1,5-PDO and 36.4% selectivity to THP (Table 2, Entry 4). The lower selectivity to 1,5-PDO than that in THFA conversion suggests that 1,2,5-PTO intermediate may be one of routes, but not the required route for the

Table 2 Results of typical compounds conversion over 4%Pt/MoS_2-FR

Entry	Reactant	Conv./%	Selectivity/%				
			1,5-PDO	THP	MTHF	Pol	Pe
1	THFA	63.7	35.4	40.4	3.5	4.3	ND
2	1,5-PDO	88.5	–	66.2	1.9	3.9	ND
3	THP	30.1	7.7	–	–	1.3	ND
4	1,2,5-PTO[b]	100	24.5	36.4	–	–	ND
5	Pol[b]	20.1	–	–	–	–	1.2

[a]Reaction conditions: 20 g 5 wt% reactant aqueous solution, 0.1 g catalyst, 4 MPa H_2, 250 °C, 8 h; ND: not detected. Conv., 1,5-PDO, THP, MTHF, Pol, Pe and 1,2,5-PTO are abbreviations for conversion, 1,5-pentanediol, tetrahydropyrane, 2-methyl tetrahydrofuran, 1-pentanol, pentane and 1,2,5-pentanetriol, respectively

[b]1 wt% solution, 1 h

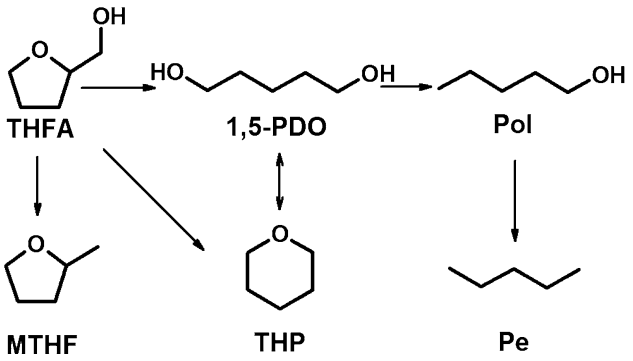

Scheme 1 Proposed reaction routes of THFA conversion over Pt/MoS_2 catalysts

1,5-PDO formation. In fact, there is no 1,2,5-PTO detected in our product solution. Therefore, the ring direct opening may be the major route for 1,5-PDO formation, as depicted in previous publications [66]. Based on the results of conditional experiments and product distribution, we proposed the reaction pathway in THFA hydrogenolysis o ver Pt/MoS_2 in Scheme 1.

4 Conclusions

MoS_2 supported noble metal catalysts were prepared for catalytic hydrogenolysis of THFA to 1,5-PDO and THP. Among the various noble metal catalysts, Pt/MoS_2 showed the relatively better catalytic performance. Over the optimal catalyst 4%Pt/MoS_2-FR, 35.4% selectivity to 1,5-PDO and 40.4% selectivity to THP were obtained at 63.7% conversion of THFA. The Pt/MoS_2 catalyst showed stable catalytic performance at least in five consecutive runs, each of which was conducted at 250 °C for 8 h in water. No leaching of Mo, S, and Pt was found during the reaction, and the crytalline structure of catalyst was retained well after reaction, consistent to the results of TPO/TPR experiments where MoS_2 and its supported noble metal catalysts showed good thermal stability under oxidative or hydrogenation atmosphere below 350 °C.

SMSI was observed between Pt and MoS_2, largely caused by the coverage of MoS_2 over Pt and rarely reported previously. The SMSI contributed to the high stability of Pt/MoS_2, and meanwhile remarkably depressed the catalytic activity for hydrogenolysis. The active sites for the reaction should be the Pt and Mo species that contacted closely. The acidity required for THFA hydrogenolysis may originate from H_2 heterolytic dissociation over Pt sites in water solution. The route of THFA hydrogenolysis over Pt/MoS_2 catalysts was proposed, where 1,5-PDO can further undergo dehydration to form THP in the reaction.

Acknowledgements This work was supported by the National Natural Science Foundation of China (21690081, 2172100028 and 21776268), "Transformational Technologies for Clean Energy and Demonstration", Strategic Priority Research Program of the Chinese Academy of Sciences, Grant XDA 21060200.

Compliance with Ethical Standards

Conflict of interest The author declare that they have no conflict of interest.

References

1. Alonso DM, Wettstein SG, Dumesic JA (2012) Bimetallic catalysts for upgrading of biomass to fuels and chemicals. Chem Soc Rev 41:8075–8098
2. Li C, Zhao X, Wang A, Huber GW, Zhang T (2015) Catalytic Transformation of Lignin for the Production of Chemicals and Fuels. Chem Rev 115:11559–11624
3. Palkovits R (2010) Pentenoic acid pathways for cellulosic biofuels. Angew Chem Int Ed 49:4336–4338

4. Huber GW, Iborra S, Corma A (2006) Synthesis of transportation fuels from biomass: chemistry, catalysts, and engineering. Chem Rev 106:4044–4098
5. Melero JA, Iglesias J, Garcia A (2012) Biomass as renewable feedstock in standard refinery units. Feasibility, opportunities and challenges. Energ Environ Sci 5:7393–7420
6. Gallezot P (2012) Conversion of biomass to selected chemical products. Chem Soc Rev 41:1538–1558
7. Tuck CO, Pérez E, Horváth IT, Sheldon RA (2012) Valorization of biomass deriving more value from waste. Science 337:695–699
8. Ruppert AM, Weinberg K, Palkovits R (2012) Hydrogenolysis goes bio: from carbohydrates and sugar alcohols to platform chemicals. Angew Chem Int Ed 51:2564–2601
9. Schlaf M (2006) Selective deoxygenation of sugar polyols to alpha, omega-diols and other oxygen content reduced materials-a new challenge to homogeneous ionic hydrogenation and hydrogenolysis catalysis. Dalton Trans. https://doi.org/10.1039/B608007C
10. Soghrati E, Choong C, Poh CK, Kawi S, Borgna A (2017) Single-Pot Conversion of Tetrahydrofurfuryl Alcohol into Tetrahydropyran over a Ni/HZSM-5 Catalyst under Aqueous-Phase Conditions. ChemCatChem 9:1402–1408
11. Tran LS, De Bruycker R, Carstensen HH, Glaude PA, Monge F, Alzueta MU, Martin RC, Battin-Leclerc F, Van Geem KM, Marin GB (2015) Pyrolysis and combustion chemistry of tetrahydropyran: Experimental and modeling study. Combust Flame 162:4283–4303
12. Tanaka H, Iwanaga Y, Wu GC, Sanui K, Ogata N (1982) Synthesis of Polyesters by Direct Polycondensation with Picryl Chloride. Polym J 8:643–648
13. Chang CC, Chen KS, Yu TL, Chen YS, Tsai CL, Tseng YH (1999) Phase segregation of polyester based-polyurethanes. Polym J 31:1205–1210
14. Mamman AS, Lee JM, Kim YC, Hwang IT, Park NJ, Hwang YK, Chang JS, Hwang JS (2008) Furfural: Hemicellulose/xylosederived biochemical. Biofuel Bioprod Bior 2:438–454
15. Xing R, Qi W, Huber GW (2011) Production of furfural and carboxylic acids from waste aqueous hemicellulose solutions from the pulp and paper and cellulosic ethanol industries. Energ Environ Sci 4:2193–2205
16. Dutta S, De S, Saha B, Alam MI (2012) Advances in conversion of hemicellulosic biomass to furfural and upgrading to biofuels. Catal Sci Technol 2:2025–2036
17. Nakagawa Y, Tamura M, Tomishige K (2015) Catalytic Conversions of Furfural to Pentanediols. Catal Surv Asia 19:249–256
18. Li X, Jia P, Wang T (2016) Furfural: A Promising Platform Compound for Sustainable Production of C4 and C5 Chemicals. ACS Catal 6:7621–7640
19. Huang KF, Brentzel ZJ, Barnett KJ, Dumesic JA, Huber GW, Maravelias CT (2017) Conversion of Furfural to 1,5-Pentanediol: Process Synthesis and Analysis. ACS Sustain Chem Eng 5:4699–4706
20. Koso S, Furikado I, Shimao A, Miyazawa T, Kunimori K, Tomishige K (2009) Chemoselective hydrogenolysis of tetrahydrofurfuryl alcohol to 1,5-pentanediol. Chem Commun. https://doi.org/10.1039/b822942b
21. Schniepp LE, Geller HH (1946) Preparation of dihydropyran delta-hydroxyvaleraldehyde and 1,5-pentanediol from tetrahydrofurfuryl alcohol. J Am Chem Soc 68:1646–1648
22. Huang KF, Won WY, Barnett KJ, Brentzel ZJ, Alonso DM, Huber GW, Dumesic JA, Maravelias CT (2018) Improving economics of lignocellulosic biofuels: An integrated strategy for coproducing 1,5-pentanediol and ethanol. Appl Energ 213:585–594
23. Tamura M, Nakagawa Y, Tomishige K (2019) Recent Developments of Heterogeneous Catalysts for Selective Hydrogenation of Unsaturated Carbonyl Compounds to Unsaturated Alcohols. J Jpn Petrol Inst 62:106–119
24. Huang RJ, Cui QQ, Yuan QQ, Wu HH, Guan YJ, Wu P (2018) Total Hydrogenation of Furfural over Pd/Al_2O_3 and Ru/ZrO_2 Mixture under Mild Conditions: Essential Role of Tetrahydrofurfural as an Intermediate and Support Effect. ACS Sustain Chem Eng 6:6957–6964
25. Amada Y, Watanabe H, Tamura M, Nakagawa Y, Okumura K, Tomishige K (2012) Structure of ReOx Clusters Attached on the Ir Metal Surface in Ir-ReOx/SiO_2 for the Hydrogenolysis Reaction. J Phys Chem C 116:23503–23514
26. Nakagawa Y, Tomishige K (2012) Production of 1,5-pentanediol from biomass via furfural and tetrahydrofurfuryl alcohol. Catal Today 195:136–143
27. Liu S, Amada Y, Tamura M, Nakagawa Y, Tomishige K (2014) One-pot selective conversion of furfural into 1,5-pentanediol over a Pd-added Ir–ReOx/SiO_2 bifunctional catalyst. Green Chem 16:617–626
28. Chen K, Mori K, Watanabe H, Nakagawa Y, Tomishige K (2012) C-O bond hydrogenolysis of cyclic ethers with OH groups over rhenium-modified supported iridium catalysts. J Catal 294:171–183
29. Tomishige K, Tamura M, Nakagawa Y (2014) Role of Re species and acid cocatalyst on Ir-ReOx /SiO_2 in the C-O hydrogenolysis of biomass-derived substrates. Chem Rec 14:1041–1054
30. Rodiansono S, Khairi T, Hara N, Ichikuni S, Shimazu, (2012) Highly efficient and selective hydrogenation of unsaturated carbonyl compounds using Ni–Sn alloy catalysts. Catal Sci Technol 2:2139
31. Pholjaroen B, Li N, Huang YQ, Li L, Wang AQ, Zhang T (2015) Selective hydrogenolysis of tetrahydrofurfuryl alcohol to 1,5-pentanediol over vanadium modified Ir/SiO_2 catalyst. Catal Today 245:93–99
32. Koso S, Ueda N, Shinmi Y, Okumura K, Kizuka T, Tomishige K (2009) Promoting effect of Mo on the hydrogenolysis of tetrahydrofurfuryl alcohol to 1,5-pentanediol over Rh/SiO_2. J Catal 267:89–92
33. Bampoulis P, Teernstra VJ, Lohse D, Zandvliet HJW, Poelsema B (2016) Hydrophobic Ice Confined between Graphene and MoS_2. J Phys Chem C 120:27079–27084
34. Dufour A, Celzard A, Fierro V, Martin E, Broust F, Zoulalian A (2008) Catalytic decomposition of methane over a wood char concurrently activated by a pyrolysis gas. Appl Catal A 346:164–173
35. Zapata PA, Faria J, Ruiz MP, Jentoft RE, Resasco DE (2012) Hydrophobic Zeolites for Biofuel Upgrading Reactions at the Liquid-Liquid Interface in Water/Oil Emulsions. J Am Chem Soc 134:8570–8578
36. Hu KH, Hu XG, Xu YF, Sun JD (2010) Synthesis of nano-MoS_2/TiO_2 composite and its catalytic degradation effect on methyl orange. J Mater Sci 45:2640–2648
37. Liang D, Gao J, Wang JH, Chen P, Hou ZY, Zheng XM (2009) Selective oxidation of glycerol in a base-free aqueous solution over different sized Pt catalysts. Catal Commun 10:1586–1590
38. Qiao B, Wang A, Yang X, Allard LF, Jiang Z, Cui Y, Liu J, Li J, Zhang T (2011) Single-atom catalysis of CO oxidation using Pt1/FeOx. Nat Chem 3:634–641
39. Lin J, Qiao B, Liu J, Huang Y, Wang A, Li L, Zhang W, Allard LF, Wang X, Zhang T (2012) Design of a highly active Ir/Fe(OH)x catalyst: versatile application of Pt-group metals for the preferential oxidation of carbon monoxide. Angew Chem Int Ed 51:2920–2924
40. Antolini E (2010) Composite materials An emerging class of fuel cell catalyst supports. Appl Catal B 100:413–426
41. Liu J (2016) Catalysis by Supported Single Metal Atoms. ACS Catal 7:34–59

42. Dosso LA, Vera CR, Grau JM (2017) Aqueous phase reforming of polyols from glucose degradation by reaction over Pt/alumina catalysts modified by Ni or Co. Int J Hydrog Energy 42:18853–18864
43. Pei WB, Dai LY, Liu YX, Deng JG, Jing L, Zhang KF, Hou ZQ, Han Z, Rastegarpanah A, Dai HX (2020) PtRu nanoparticles partially embedded in the 3DOM $Ce_{0.7}Zr_{0.3}O_2$ skeleton: Active and stable catalysts for toluene combustion. J Catal 385:274–288
44. Sun SH (2006) Recent advances in chemical synthesis, self-assembly, and applications of FePt nanoparticles. Adv Mater 18:393–403
45. Liu XY, Liu MH, Luo YC, Mou CY, Lin SD, Cheng HK, Chen JM, Lee JF, Lin TS (2012) Strong Metal-Support Interactions between Gold Nanoparticles and ZnO Nanorods in CO Oxidation. J Am Chem Soc 134:10251–10258
46. Britvin SN, Kashtanov SA, Krivovichev SV, Chukanov NV (2016) Xenon in Rigid Oxide Frameworks: Structure, Bonding and Explosive Properties of Layered Perovskite $K_4Xe_3O_{12}$. J Am Chem Soc 138:13838–13841
47. Tauster SJ, Fung SC, Garten RL (1978) Strong metal-support interactions : Group 8 noble metals supported on titanium dioxide. J Am Chem Soc 100:170–175
48. Han B, Guo YL, Huang YK, Xi W, Xu J, Luo J, Qi HF, Ren YJ, Liu XY, Qiao BT, Zhang T (2020) Strong Metal-Support Interactions between Pt Single Atoms and TiO_2. Angew Chem Int Ed 59:11824–11829
49. Yan QQ, Wu DX, Chu SQ, Chen ZQ, Lin Y, Chen MX, Zhang J, Wu XJ, Liang HW (2019) Reversing the charge transfer between platinum and sulfur-doped carbon support for electrocatalytic hydrogen evolution. Nat Commun 10:4977–4985
50. Tang HL, Su Y, Zhang BS, Lee AF, Isaacs MA, Wilson K, Li L, Ren YG, Huang JH, Haruta M, Qiao BT, Liu X, Jin CZ, Su DS, Wang JH, Zhang T (2017) Classical strong metal–support interactions between gold nanoparticles and titanium dioxide. Sci Adv 3:e1700231
51. Tang H, Liu F, Wei J, Qiao B, Zhao K, Su Y, Jin C, Li L, Liu JJ, Wang J, Zhang T (2016) Ultrastable Hydroxyapatite/Titanium-Dioxide-Supported Gold Nanocatalyst with Strong Metal-Support Interaction for Carbon Monoxide Oxidation. Angew Chem Int Ed 55:10606–10611
52. Xiao Y, Zhang E, Zhang J, Dai Y, Yang Z, Christensen HEM, Ulstrup J, Zhao F (2017) Extracellular polymeric substances are transient media for microbial extracellular electron transfer. Sci Adv 3:e1700623
53. Li H, Zhang Q, Yap CCR, Tay BK, Edwin THT, Olivier A, Baillargeat D (2012) From Bulk to Monolayer MoS_2: Evolution of Raman Scattering. Adv Funct Mater 22:1385–1390
54. Baker MA, Gilmore R, Lenardi C, Gissler W (1999) XPS investigation of preferential sputtering of S from MoS_2 and determination of MoSx stoichiometry from Mo and S peak positions. Appl Surf Sci 150:255–262
55. Xiao B, Zheng MY, Li XS, Pang JF, Sun RY, Wang H, Pang XL, Wang AQ, Wang XD, Zhang T (2016) Synthesis of 1,6-hexanediol from HMF over double-layered catalysts of Pd/SiO_2 + Ir-ReOx/SiO_2 in a fixed-bed reactor. Green Chem 18:2175–2184
56. Tamura M, Amada Y, Liu SB, Yuan ZL, Nakagawa Y, Tomishige K (2014) Promoting effect of Ru on Ir-ReOx/SiO_2 catalyst in hydrogenolysis of glycerol. J Mol Catal A 388:177–187
57. Wang J, Zhao X, Lei N, Li L, Zhang L, Xu S, Miao S, Pan X, Wang A, Zhang T (2016) Hydrogenolysis of Glycerol to 1,3-propanediol under Low Hydrogen Pressure over WOx-Supported Single/Pseudo-Single Atom Pt Catalyst. Chemsuschem 9:784–790
58. Umbarkar SB, Biradar AV, Mathew SM, Shelke SB, Malshe KM, Patil PT, Dagde SP, Niphadkar SP, Dongare MK (2006) Vapor phase nitration of benzene using mesoporous MoO_3/SiO_2 solid acid catalyst. Green Chem 8:488–493
59. Zhao X, Wang J, Yang M, Lei N, Li L, Hou B, Miao S, Pan X, Wang A, Zhang T (2017) Selective Hydrogenolysis of Glycerol to 1,3-Propanediol: Manipulating the Frustrated Lewis Pairs by Introducing Gold to Pt/WOx. Chemsuschem 10:819–824
60. Doudin N, Yuk SF, Marcinkowski MD, Nguyen MT, Dohnalek Z (2019) Understanding Heterolytic H2 Cleavage and Water-Assisted Hydrogen Spillover on Fe_3O_4(001)-Supported Single Palladium Atoms. ACS Catal 9:7876–7887
61. Nakagawa Y, Mori K, Chen K, Amada Y, Tamura M, Tomishige K (2013) Hydrogenolysis of C-O bond over Re-modified Ir catalyst in alkane solvent. Appl Catal A 468:418–425
62. He JY, Burt SP, Ball MR, Hermans IAC, Dumesic JA, Huber GW (2019) Catalytic C-O bond hydrogenolysis of tetrahydrofuran-dimethanol over metal supported WOx/TiO_2 catalysts. Appl Catal B 258:117945–117954
63. Du X, Huang Y, Pan X, Han B, Su Y, Jiang Q, Li M, Tang H, Li G, Qiao B (2020) Size-dependent strong metal-support interaction in TiO_2 supported Au nanocatalysts. Nat Commun 11:5811
64. Liu SB, Amada Y, Tamura M, Nakagawa Y, Tomishige K (2014) Performance and characterization of rhenium-modified Rh-Ir alloy catalyst for one-pot conversion of furfural into 1,5-pentanediol. Catal Sci Technol 4:2535–2549
65. Koso S, Nakagawa Y, Tomishige K (2011) Mechanism of the hydrogenolysis of ethers over silica-supported rhodium catalyst modified with rhenium oxide. J Catal 280:221–229
66. Nakagawa Y, Tamura M, Tomishige K (2013) Catalytic Reduction of Biomass-Derived Furanic Compounds with Hydrogen. ACS Catal 3:2655–2668